Nanoscale Silicon Oxide Reduces Electron Transfer Kinetics of Surface-Bound Ferrocene Monolayers on Silicon

Tiexin Li[1], Essam M. Dief, [1] Xin Lyu,[1] Soraya Rahpeima,[1] Simone Ciampi[1], Nadim Darwish[1]*

[1]*School of Molecular and Life Sciences, Curtin University, Bentley, WA 6102, Australia*

Corresponding author: nadim.darwish@curtin.edu.au

KEYWORDS: Self-assembled monolayers, ferrocene, molecule-electrode contact, silicon oxidation, electron transfer kinetics

Abstract

Functionalising Si with self-assembled monolayers (SAMs) paves the way for integrating the semiconducting properties of Si with the diverse properties of organic molecules. Highly packed SAMs such as those formed from alkyl chains are desired to protect Si from re-oxidation in ambient environment. Such monolayers have been largely considered oxide-free but the effect of nanoscale re-oxidation on the electrochemical kinetics of Si-based SAMs remains unknown. Here, we systematically study the effect of the oxide growth on the electrochemical charge-transfer kinetics of ferrocene-terminated SAMs on Si by exposing the surfaces to ambient conditions for controlled periods of time. X-ray photoelectron spectroscopy and atomic force microscopy revealed a gradual growth of silicon oxide (SiO_x) on the surfaces over time. The oxide growth is accompanied by a decrease in the ferrocene surface coverage and a concomitant decrease in the electron transfer rate constant (k_{et}) measured by electrochemical impedance spectroscopy. The drop in k_{et} is attributed to a greater spacing between the ferrocene moieties induced by the surface oxide, which in turn blocks lateral electron transfer between neighbouring ferrocene moieties. These findings explain the highly scattered literature data on electron-transfer kinetics for

monolayers on Si and have implications for the proper design of Si-based molecular electronics devices.

1. Introduction

Fundamental and applied research on the self-assembly of organic molecules on electrode surfaces continues to be an area of intense research. To date, the focus has been on the formation of self-assembled monolayers (SAMs) on gold electrodes using thiol or disulfide-terminated molecules.[1-11] but there is increasing interest of forming monolayers on a range of other electrodes.[12-14] The work of Chidsey and co-workers on Si–C-bound monolayers has helped to expand this research from metals to semiconductors.[15-17] In particular, monolayers on oxide-free silicon (Si–H) have gained significant interest because they enable combining the traditional semiconducting properties of Si with that of functional organic molecules.[15, 18-27] For example, Si-based SAMs have been exploited in solar cells research,[28-30] biosensors,[31-34] fundamental electron transfer studies[35-37] and molecular electronics.[38-42]

The formation of SAMs on Si–H, however, is not as straightforward as that formed on gold or other metal electrodes.[6, 24, 43] The first step in forming SAMs on Si requires etching away the insulating oxide (SiO_x) layer,[15, 44-47] using fluoride solutions, resulting in a reactive Si–H surface that starts re-oxidizing almost immediately under ambient conditions.[45, 48-49] Therefore most procedures for preparing SAMs on Si require rapidly reacting a freshly prepared Si–H surfaces with organic molecules to form SAMs in an oxygen-free environment.[50-51] After the formation of a SAM, the surface is free of oxide. What is not known is how effective these monolayers are in preventing re-oxidation of the Si surface. Conventional surface spectroscopies, such as XPS, tend to underestimate the oxide content. It is important to detect early stages of oxidation since small island of silica will inevitably expand over time. The quality of the SAMs is key in defining the

interfacial electrical properties of the functionalised Si–H surface. Therefore, highly packed monolayers are desired to prevent ambient oxidising agents (water and oxygen) from penetrating the molecular film and re-oxidising the Si.[52] Although, functionalising Si–H surfaces with alkyne-terminated monolayers using UV light or heat have led to densely-packed SAMs, the maximum coverage of high-quality alkyne-based monolayers are 60–65% of the total reactive Si–H surface sites.[53-54] Therefore 35% of the Si–H surface remain prone to oxidation upon exposure to water or oxygen.[55-56] The growth of SiO_x has been speculated to increase or decrease charge transfer kinetics and published data on redox kinetics of Si are highly scattered and the factors contributing to the irreproducibility remains largely unknown.[52, 57-58]

Here, we systematically study the effect of surface oxide growth on the charge transfer kinetics of Si-based SAMs. We investigate under ambient conditions (21 ℃ and 30% relative humidity) the stability and the electrochemical performance of an alkyne-terminated SAMs formed on a freshly etched Si–H surface. The charge transfer kinetics was studied on SAMs functionalized with a terminal ferrocene moiety using cyclic voltammetry (CV) and electrochemical impedance spectroscopy (EIS). Atomic force microscopy (AFM) and X-ray photoelectron spectroscopy (XPS) were utilized to visualize the nanoscale SiO_x growth over time. We used two procedures: a) using a SAM composed of an alkane chain (nonadiyne) that is grafted by hydrosilylation reaction followed by a copper-catalysed "click" reaction with an azidomethylferrocene (Figure 1). The formed ferrocene-terminated SAM is then exposed to ambient conditions for specific period of times while the charge transfer kinetics is monitored and (b) preparing a SAM of nonadiyne which is then left for specific periods of time at ambient conditions. The SAM's terminal alkynes are then reacted with azidomethylferrocene and the charge transfer kinetics of the redox SAM formed, is monitored.

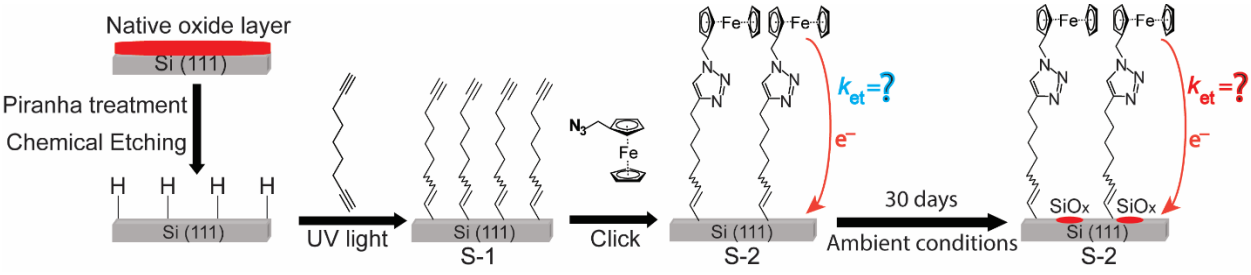

Figure 1. Schematic of the SAMs studied. Oxide-free silicon (Si–H) electrodes are reacted with 1,8-nonadiyne via a hydrosilylation reaction to form SAM **S-1**. A ferrocene moiety is attached to the distal end of the monolayer by a copper-catalyzed azide-alkyne "click" reaction to yield the redox-active SAM **S-2**.

2. MATERIALS AND METHODS

2.1 Materials. Unless specified otherwise, all chemicals were of analytical grade and used as received. Chemicals used in surface modification and electrochemical experiments were of high purity (>99%). Milli-Q water (>18 MΩ cm) was used for surface cleaning, glassware cleaning and for the preparation of the electrolyte solutions. Dichloromethane (DCM) and 2-propanol were distilled before use. Hydrogen peroxide (30 wt% in water), sulfuric acid (Puranal TM, 95-97%) and ammonium fluoride (Puranal TM, 40 wt% in water) were of semiconductor grade and were used for silicon wafer cleaning and etching. 1,8-Nonadiyne (98%) was obtained from Sigma-Aldrich and used as received. Azidomethylferrocene was synthesised from ferrocene methanol using a literature procedure.[59] Aqueous perchloric acid (1.0 M) was used as the electrolyte in all electrochemical measurements. Silicon wafers were purchased from Siltronix, S.A.S. (Archamps, France), p-type boron doped, and had a thickness of 500 ± 25 μm and a resistivity of 0.007–0.013 Ω cm.

2.2 Surface Modification

2.2.1 Silicon Passivation. The hydrosilylation reaction of 1,8-nonadiyne with Si–H followed a previously reported procedure.[60-61] In brief, silicon wafers were cut into pieces (approximately 1 × 1 cm), cleaned in hot Piranha solution (130 °C, 3:1(v/v) mixture of concentrated sulfuric acid to 30% hydrogen peroxide) for 20 minutes, then rinsed with water and etched in deoxygenated (40 wt%) aqueous ammonium fluoride solution under a stream of argon for 13 minutes. The etched samples were rinsed with Milli-Q water and DCM before being placed in a deoxygenated sample of 1,8-nonadiyne. The surfaces were then rapidly transferred to a reaction chamber kept under nitrogen flow, and illuminated with UV light (Vilber, VL-215.M, $\lambda = 312$ nm) for 2 hours.

2.2.2 Copper-catalysed azide–alkyne "click" reaction. The 1,8-nonadiyne SAMs (**S-1**, Figure 1) were reacted with azidomethylferrocene through a copper-catalysed "click" reaction. In brief, **S-1** samples were incubated in a solution of 0.4 μM copper (II) sulphate pentahydrate, sodium ascorbate (5 mg/mL) and 0.5 mM azidomethylferrocene, under dark conditions. The reaction time was varied between 1 and 60 minutes. The silicon substrates were then removed from the solution and washed sequentially with 2-propanol, Milli-Q water, 0.5 M hydrochloric acid, Milli-Q water, 2-propanol and DCM. Finally, the silicon substrates (**S-2**) were blown dry with a stream of argon before analysis.

To study the effect of surface oxidation on electrode kinetics, two procedures were used. **S-2** samples were either exposed to ambient conditions (21 °C and 30% relative humidity) for 1–30 days, or **S-1** samples were kept under ambient conditions for 1–15 days prior to the click reaction

2.3. Surface characterization

2.3.1 Electrochemical measurements. Electrochemical measurements were carried out in a single-compartment, three-electrode PTFE cell using a CHI650 electrochemical workstation (CH Instruments, USA). The modified silicon surface (**S-2**) served as the working electrode, a platinum wire as the auxiliary electrode, and an Ag/AgCl aqueous electrode (1.0 M KCl, CH Instruments, USA) as the reference electrode. Aqueous 1.0 M perchloric acid was used as the electrolyte. The electrical contact between silicon and copper was reached by rapidly rubbing gallium indium eutectic on the back side of the silicon substrate. All CVs are started anodically from 0 V to 0.8 V and reversed back to 0 V. EIS measurements were carried out at a DC offset equal to the half-wave potential ($E_{1/2}$) measured in the CV experiments. The AC amplitude was 15 mV and the frequency was scanned between 4 and 100,000 Hz. The surface coverages (Γ) of ferrocene molecules was calculated from the integration of the CV oxidation waves according to $\Gamma=Q/nFA$ (where Q is charge, n is number of electron transfer, F is Faraday constant and A is area of electrode).

2.3.2 X-Ray Photoelectron Spectroscopy (XPS) measurements. XPS spectra were obtained on an AXIS Ultra DLD spectrometer (Kratos Analytical Ltd) with a monochromatic Al Kα source (1486.7 eV), an imaging hemispherical analyser and a 6 channel detector. Spectra were recorded in normal emission with the analysing chamber operating below 10^{-9} mbar. The resolution of the spectrometer is ca. 0.6 eV, the step size was 0.1 eV, the dwell time 100 ms, and an analyser pass energy was set to 20 eV. The spectra were processed in CasaXPS software using the Shirley background subtraction. All binding energies are expressed in eV and were corrected by adjusting the main C1s signal to 284.7 eV.

2.3.3 Atomic Force Microscopy (AFM). AFM topography imaging was conducted on a Park AFM NX10 (Park Systems, Korea) in air and at room temperature using silicon tips (OMCL-

AC160TS, Olympus), with spring constant of 26 N/m and resonance frequency of 300 kHz. AFM data was processed with Park Systems XEI 4.3.4. Measurements were performed in tapping mode with the image size set to 5×5 µm, the resolution to 256 points/line and the scan rate to 0.5 Hz.

3. RESULTS AND DISCUSSION

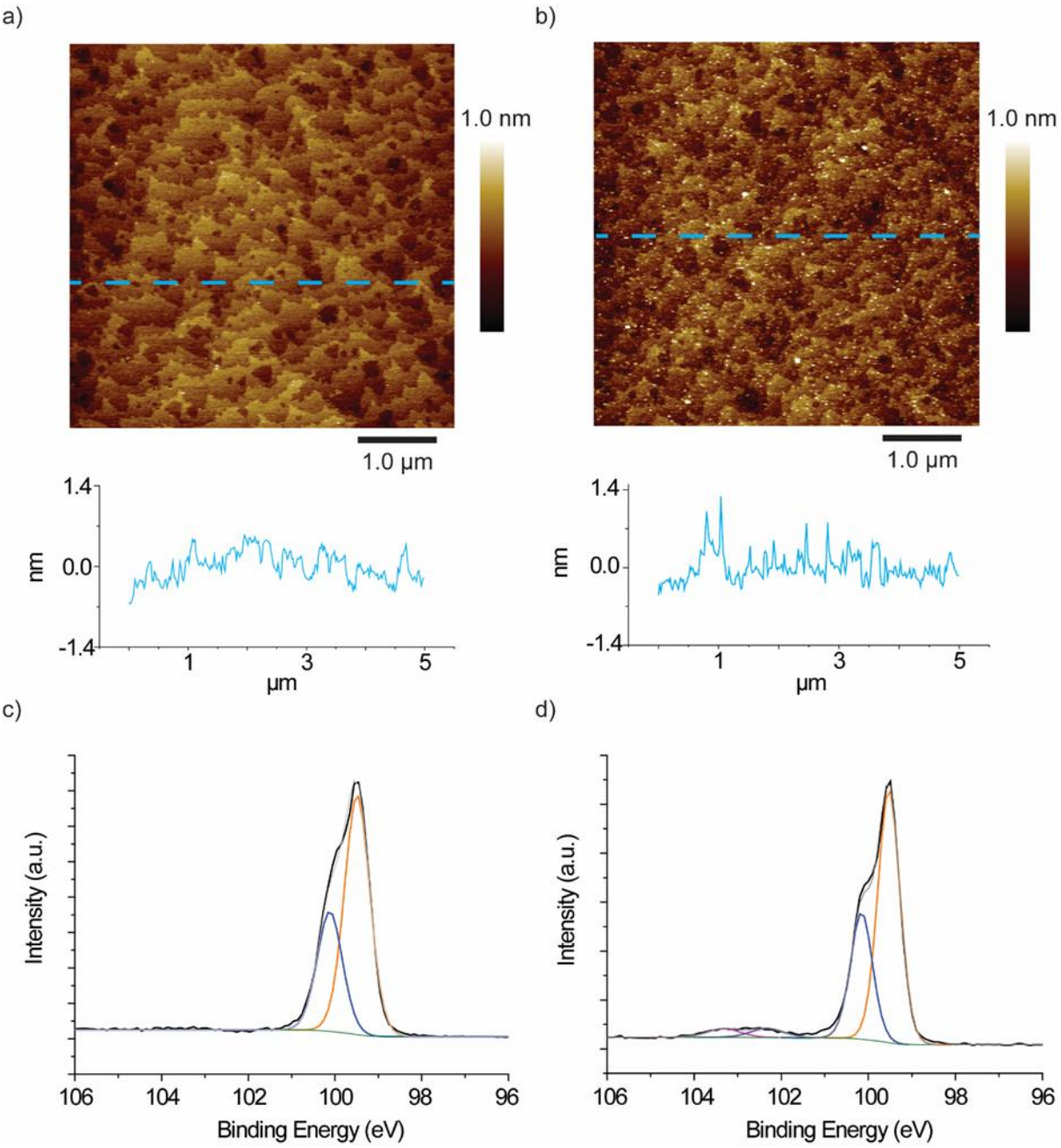

Figure 2. a) AFM topography images for **S-1** SAM in day 1. b) AFM topography images for an **S-1** SAM left at ambient conditions for 15 days, showing oxide growth appearing as white spots in the topography images and the Si (111) terraces become less sharp. The inset in (a) and (b) show cross-sectional profile (line) roughness of the **S-1** SAM at day 1 and 15 days, respectively. The cross-sectional roughness of the Si–H surface are shown in the inset of Figure S1 (Supporting Information). c) XPS High resolution Si 2p spectra for **S-1** SAM in day 1, d) XPS High resolution Si 2p spectra for monolayer of **S-1** SAM in day 15. The absence of emission at 103 eV in day 1 indicates that there is no detectable oxide formed in short period. By exposing the surface to ambient conditions for 15 days, a SiO_x emission of 3% relative to the Si 2p appears at 103 eV.

AFM topography imaging of the surface **S-1** on day 1 shows clearly visible flat terraces with smooth edges, peak-to-peak surface roughness within individual terrace of ~0.213 nm, and negligible oxide (Figure 2a). Figure 2b shows topography images acquired for samples aged 15 days under ambient conditions, and here the surface shows clear oxide spots (rounded features) and the Si(111) terraces become less visible. The amount of oxide increases with time, even though the Si–H surfaces were oxide-free after etching and before the hydrosilylation with 1,8-nonadiyne (Figure S1). The silicon used in this experiment is p-type silicon which have a single crystalline orientation on the (111) plane. The AFM images show the terraces of the (111) plane for bare Si–H surface (Figure S1a) and fresh 1,8 nonadiyne-functionalised Si surface (Figure 2a). The root mean square roughness (RMS) of the Si–H and fresh 1,8 nonadiyne-functionalised Si surfaces are both similar at 0.20 nm (inset in Figure 2 and Figure S1a , Supporting Information). On the other hand, the oxidized 1,8 nonadiyne-functionalised Si-surface showed a higher RMS roughness of 0.25 nm (Figure 2b). On day 1, XPS Si 2p narrow scan of surface **S-1** show no significant oxide or suboxide (Figure 2c).[62] The Si 2p high resolution envelope was fitted by two peaks, with the main emission composed of one spin-orbit split with two peaks at 99.5 eV and 100.1 eV, corresponding to the Si $2p_{3/2}$ and Si $2p_{1/2}$ for low and high energy spins, respectively. For the surface **S-1** on day 15, the Si 2p high resolution envelope shows three peaks, with the main emission composed of one spin–orbit-split with two peaks at 99.5 eV and 100.1 eV, corresponding

to the Si $2p_{3/2}$ and Si $2p_{1/2}$ for low and high energy spins, respectively. The new peak at 102.7 eV is assigned to SiO_x bonding (Figure 2d). The C 1s signal from the freshly prepared monolayer (1day) shows C–C bonding ascribed to the methylene carbon at 285.0 eV while the peak at 283.6 eV is ascribed to the olefinic carbon that is bound to Si as Si–C=C and the emission at 286.5 eV is ascribed to carbon–oxygen bonding (C–O). Oxygen contamination has been observed in many reports and are present in the form of CO_2, explaining the appearance of some oxygen bound to carbon in the C 1s emisssion.[63-64] Figure S2d, shows the C 1s emission from the surface **S-1** after 15 days at ambient conditions. The peak at 285.0 eV is ascribed to the C–C bonding, the peak at 283.6 eV to the Si–C=C bonding and the peaks between 286 and 290 eV to carbon that is bound to oxygen. The survey XPS spectra of **S-1** SAM in day 1 and day 15 are shown in Figure S2 (Supporting Information). The XPS result for SAM **S-2** is shown in Figure S13 (Supporting Information).

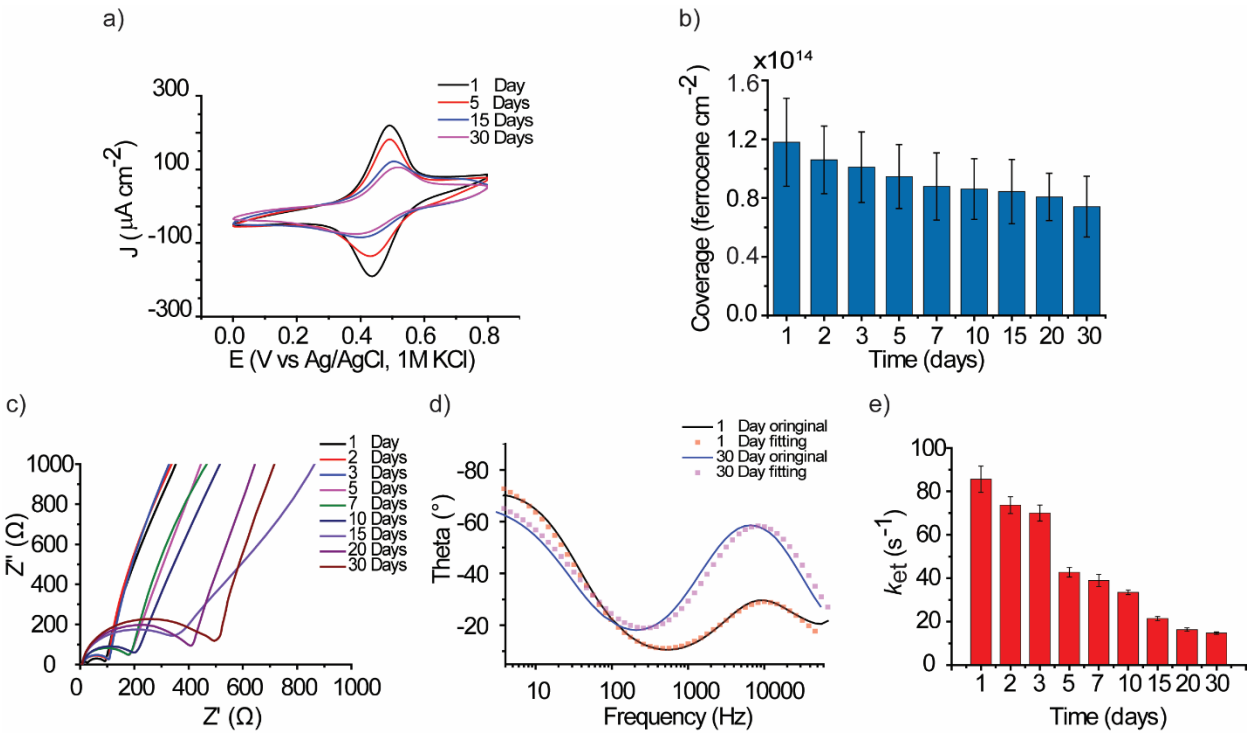

Figure 3. Electrochemical characterisation of SAM **S-2** in which the click reaction was performed at day 1 followed by the exposure period. a) The corresponding CVs at day 1, 5, 15, and 30 days. b) The corresponding surface coverages calculated from the oxidation waves of the CVs in (a). c) Nyquist plots from EIS measurements for 1 exposure day (black), 2 days (red), 3 days (blue), 5 days (magenta), 7 days (olive), 10 days (navy), 15 days (violet), 20 days (purple), and 30 days (wine). d) Bode plots for day 1 and 30 with frequency range from 4 Hz to 60000 Hz. Lines (black and blue) are experimental data and scattered dots (red and magenta) are best fit to the experimental data. Bode plots for other exposure periods are shown in Figure S3c and S6, of Supporting Information. e) The evolution of k_{et} obtained by fitting the impedance data to Randles Circuit (Table S2, Supporting Information). The error bars in (b) and (e) are the standard deviation of surface coverages and k_{et} values from the mean value of three different surfaces.

Figure 3a shows the CVs for **S-2** SAM after resting the surfaces at ambient condition for different times ranging from 1 to 30 days. The CVs show the characteristic redox peaks of the ferrocene moiety at 0.46 V vs Ag/AgCl. The first key observation from the CVs is the decrease in the ferrocene surface coverage with increasing exposure time. This is inferred by observing a decrease in the peak current for both the oxidation and reduction waves with time. The coverage decrease by ~ 37% from $(1.18 \pm 0.30) \times 10^{14}$ ferrocene cm^{-2} at day 1, to $(7.41 \pm 2.07) \times 10^{13}$ ferrocene cm^{-2} at day 30 (Figure 3b). This is accompanied by an incresed separation between the oxidation and reduction waves. At day 1, the waves are only separated by 50 mV, but this gap increased to 140 mV at day 30 – indicating a slower electron transfer kinetics. CVs for individual exposure periods are shown in Figure S3 and S4 (Supporting Information).

To assess the charge transfer kinetics, electrochemical impedance spectroscopy (EIS) was performed on SAM **S-2**. The Nyquist and the Bode plots in Figure 3c and 3d, visually indicate that the resistance of the monolayer increases with the increase in the exposure time. For instance, the progressive increase in the diameter of the semicircle on the real component of the impedance (x-axis in Figure 3c) reflect the progressive increase in the resistance of the monolayer. Similarly, the shift from a higher to a lower frequency at which the dip in the phase angle (Bode plot in Figure 3d) appears is an indication of a slower electron transfer kinetics with exposure time. Full

description of the impedance spectra can be found in previous literature.[65-68] The equivalent circuit used to fit the EIS data are shown in Figure S7 (Supporting Information). The k_{et} decreases with the waiting time (Figure 3e). The k_{et} decrease from (85.64 ± 6.06) s^{-1} on day 1 to (14.74 ± 0.54) s^{-1} on day 30. A similar trend for the decrease in k_{et} was observed by using the Laviron approach of calculating k_{et} from the CVs (Figure S12, Supporting Information). This trend appears to be related to the decrease in the surface coverage which in turn, appears to be related to the amount of surface oxides on the surface.[69] Nyquist plots for individual exposure periods are shown in Figure S5 (Supporting Information).

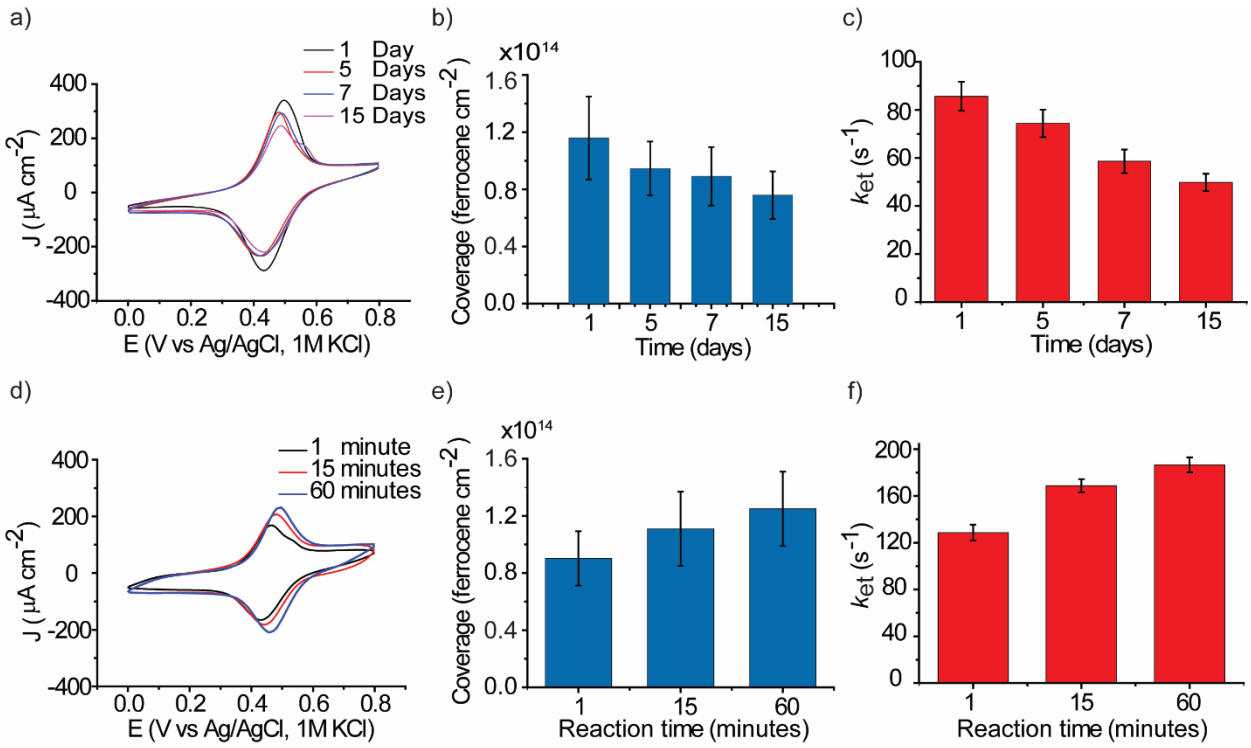

Figure 4. a) CVs for SAM **S-2** at different exposure periods which is applied to the nonadiyne SAM (**S-1**) before performing the click reaction. The surfaces were left at ambient conditions for 5, 7, and 15 days and the click reaction was freshly performed on the day the CVs were measured. The CV corresponding to 1 exposure day is shown in black, 5 days (red), 7 days (blue), and 15 days (magenta). b) Evolution of ferrocene surface coverage of SAM **S-2** versus the exposure time. c) The evolution in k_{et} at different exposure periods. d) CVs for a freshly prepared SAM **S-2** with different duration of the click reaction. The surfaces were left in the click reaction solution for 1 minute (black), 15 minutes (red), and 60 minutes (blue). e) The corresponding surface coverage of

ferrocene at different click reaction times. f) Evolution of k_{et} for different click reaction times. The error bars in (b), (c), (e), and (f) are the standard deviation of surface coverages and k_{et} from the mean value of three different surfaces.

To test whether the decrease in the surface coverage is due surface oxidation or decomposition of the ferrocene moieties with time, we performed similar experiments but instead of applying the exposure periods to the ferrocene terminated monolayers, they were applied to the base 1,8-nonadiyne monolayer (**S-1**) while the click reaction with azidomethylferrocene was only performed after the exposure period. This ensured that the ferrocene moieties are protected from aging and enabled investigating whether or not the decrease in surface coverage is related to decomposition of the ferrocene moieties. (Figure 4a, b) Results showed a similar trend to that observed with pre-clicked surfaces (**S-2**) with the k_{et} decreasing with the exposure period (Figure 4c). This indicates that the decrease in k_{et} is affecting the base nonadiyne monolayer, most likely due to the formation of SiO_x which partially desorbs some of the monolayer. This is consistent with the AFM and XPS results (Figure 2) which showed that SiO_x grows with time. It is worth re-emphasizing that the click reaction here is only preformed after the oxidation of the nonadiyne monolayer. Observing the same trend in surface coverage and k_{et} to that of the pre-clicked surfaces (Figure 3b, e) indicates that it is likely that the nonadiyne molecules are desorbing from the surface rather than the oxide reducing the amount of electrochemically active ferrocenes. CVs for individual exposure periods are shown in Figure S8 (Supporting Information) while Figure S9 shows the Nyquist plots for individual exposure periods.

Next, we investigated the reason behind the decrease in the kinetics of electron transfer. Is it due the presence of silicon oxide and its nature as an electrical insulator or is it due the lower ferrocene coverage which increases the distance between the ferrocene moieties? For this purpose, we performed experiments in which the surface coverage of the ferrocene moieties are controlled

without oxidizing the surface and, therefore, without exposure periods to ambient conditions. This was performed by controlling the azide-alkyne click reaction times on a freshly prepared nonadiyne surface. The surface coverage obtained following this procedure ranged from (9.03 ± 1.90)×10^{13} to (1.25 ± 0.26) ×10^{14} ferrocene cm^{-2} for click reaction time of 1 and 60 minutes, respectively (Figure 4e). CVs for other click reaction time are shown in Figure S11 (Supporting Information). Electrochemical impedance measurements showed an increase in k_{et} from (128.66 ± 6.78) s^{-1} to (186.57 ± 6.49) s^{-1} as a function of the increase in surface coverage (Figure 4f). This trend is similar to that observed for the oxidized surface studies and indicates that the reason behind the decrease in k_{et} is most likely due to the surface oxide creating a less dense ferrocene monolayer on the surface, as distinct from the effect of the insulating properties of the oxide itself (Figure 5). The model (Figure 5) is not proven experimentally; and assumes that the oxide grow progressively from the molecular scale to the nanoscale and then to the microscale. Therefore, it is likely that some oxide comparable to the dimension of the molecules are present on the surface. Nyquist plots and Bode plots for individual click reaction times are shown in Figure S10 and S11 (Supporting Information).

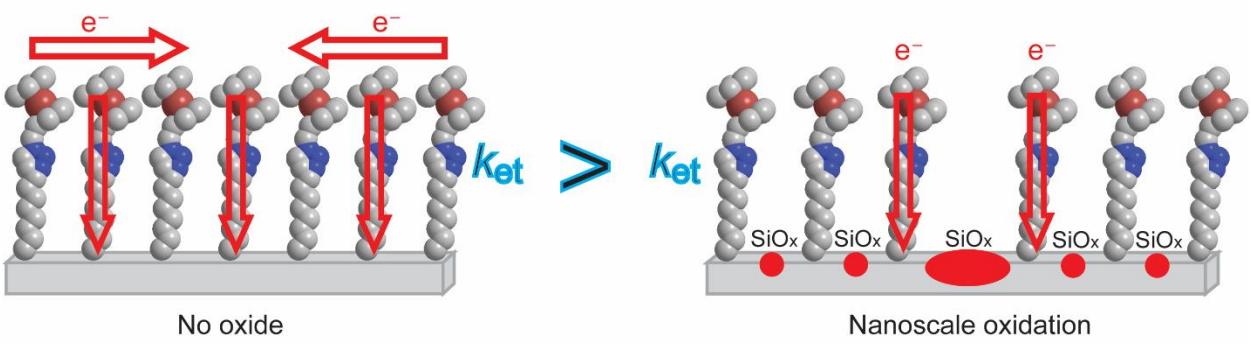

Figure 5. A simplified model on the proposed impact of silicon oxide on the kinetics of electron transfer through redox monolayers on silicon electrodes. The nanoscale oxidation leads to partial monolayer desorption and a lower density of ferrocenes on the surface which reduces lateral electron transfer between the ferrocene moieties that, in turn, reduces the overall electron transfer kinetics. The model assume that oxide smaller than the dimension of the molecules, which is below the resolution of the AFM images, is present on the surface. Small oxide spots separate individual

ferrocene molecules from each other. Larger oxide protrusions will separate cluster of ferrocene molecules from other clusters. The overall effect is a reduction in the lateral electron transfer between ferrocene moieties. The oxide spots are not drawn to scale.

4. CONCLUSIONS

In summary, we demonstrate that the growth of nanoscale oxide on monolayer-covered Si surfaces has profound effect on the surface coverage of the monolayers, and as a result, on the electron transfer kinetics across the monolayer. Early oxide growth that is not detectable by XPS, nor by more sensitive AFM imaging, has a dramatic effect on electrode kinetics. After 15 days at ambient conditions, oxide growth on nonadiyne-covered Si surfaces become detectable by AFM and XPS. After 30 days, the electron transfer rate constant k_{et} decreases by 4-folds compared to the same SAMs at day 1. The oxide growth is accompanied by a decrease in the surface coverage of the molecules forming the SAM and this is attributed to the oxide partially desorbing the monolayer and creating defects. The decrease in the electron transfer kinetics is attributed to the lower density of ferrocene on the surface which diminish lateral electron transfer that is responsible for the high electron transfer kinetics reported in literature for high-density ferrocene monolayers.[42] These results explain the largely variable electron transfer kinetics reported on silicon and demonstrate the need to take into consideration the effect of oxide growth on the performance of Si-based monolayers for a range of applications. The approach may also be used as an early silicon oxide detection that is below the detection limit of common surface spectroscopy and microscopy techniques.

SUPPORTING INFORMATION

Detailed AFM, XPS and electrochemical analysis are supplied as Supporting Information.

DECLARATION OF COMPETING INTEREST

The authors declare no competing financial interest.

ACKOWLEDGEMENTS

The authors acknowledge support from the Australian Research Council (DP190100735).

5. REFERENCES

1. Xia, Y.; Rogers, J. A.; Paul, K. E.; Whitesides, G. M., Unconventional Methods for Fabricating and Patterning Nanostructures. *Chem. Rev.* **1999**, *99*, 1823-1848.

2. Darwish, N.; Díez-Pérez, I.; Da Silva, P.; Tao, N.; Gooding, J. J.; Paddon-Row, M. N., Observation of Electrochemically Controlled Quantum Interference in a Single Anthraquinone-Based Norbornylogous Bridge Molecule. *Angew. Chem. Int. Ed.* **2012**, *51*, 3203-3206.

3. Gooding, J. J.; Darwish, N., The Rise of Self-Assembled Monolayers for Fabricating Electrochemical Biosensors—an Interfacial Perspective. *Chem. Rec.* **2012**, *12*, 92-105.

4. Darwish, N.; Eggers, P. K.; Ciampi, S.; Tong, Y.; Ye, S.; Paddon-Row, M. N.; Gooding, J. J., Probing the Effect of the Solution Environment around Redox-Active Moieties Using Rigid Anthraquinone Terminated Molecular Rulers. *J. Am. Chem. Soc.* **2012**, *134*, 18401-18409.

5. Pla-Vilanova, P.; Aragonès, A. C.; Ciampi, S.; Sanz, F.; Darwish, N.; Diez-Perez, I., The Spontaneous Formation of Single-Molecule Junctions Via Terminal Alkynes. *Nanotechnology* **2015**, *26*, 381001.

6. Darwish, N.; Eggers, P. K.; Ciampi, S.; Zhang, Y.; Tong, Y.; Ye, S.; Paddon-Row, M. N.; Gooding, J. J., Reversible Potential-Induced Structural Changes of Alkanethiol Monolayers on Gold Surfaces. *Electrochem. Commun.* **2011**, *13*, 387-390.

7. Walkey, M. C.; Peiris, C. R.; Ciampi, S.; C. Aragonès, A.; Domínguez-Espíndola, R. B.; Jago, D.; Pulbrook, T.; Skelton, B. W.; Sobolev, A. N.; Díez Pérez, I., Chemically and Mechanically Controlled Single-Molecule Switches Using Spiropyrans. *ACS Appl. Mater. Interfaces* **2019**, *11*, 36886-36894.

8. Zhang, H.-X.; Sasaki, Y.; Abe, M.; Zhang, Y.; Ye, S.; Osawa, M.; Uosaki, K., Electrochemical and Infrared Spectroscopic Study of the Self-Assembled Monolayer of a Cyano-Bridged Dimeric Triruthenium Complex on Gold Surface. *J. Electroanal. Chem.* **2014**, *714*, 51-55.

9. Zhang, L.-Y.; Zhang, H.-X.; Ye, S.; Wen, H.-M.; Chen, Z.-N.; Osawa, M.; Uosaki, K.; Sasaki, Y., A Butadiyne-Linked Diruthenium Molecular Wire Self-Assembled on a Gold Electrode Surface. *Chem. Commun.* **2011**, *47*, 923-925.

10. Sieval, A. B.; Linke, R.; Zuilhof, H.; Sudhölter, E. J., High-Quality Alkyl Monolayers on Silicon Surfaces. *Adv. Mater.* **2000**, *12*, 1457-1460.

11. Aragonès, A. C.; Darwish, N.; Ciampi, S.; Jiang, L.; Roesch, R.; Ruiz, E.; Nijhuis, C. A.; Díez-Pérez, I., Control over near-Ballistic Electron Transport through Formation of Parallel Pathways in a Single-Molecule Wire. *J. Am. Chem. Soc.* **2018**, *141*, 240-250.

12. Gautam, R. P.; Barile, C. J., Preparation and Electron-Transfer Properties of Self-Assembled Monolayers of Ferrocene on Carbon Electrodes. *J. Phys. Chem. C* **2021**, *125*, 8177-8184.

13. Dief, E. M.; Darwish, N., Ultrasonic Generation of Thiyl Radicals: A General Method of Rapidly Connecting Molecules to a Range of Electrodes for Electrochemical and Molecular Electronics Applications. *ACS Sens.* **2020**, *6*, 573-580.

14. Reimers, J. R.; Wang, Y.; Kosov, D. S., Decomposition of Ferrocene on Pt (111) and Its Effect on Molecular Electronic Junctions. *J. Phys. Chem. C* **2019**, *123*, 15569-15574.

15. Linford, M. R.; Fenter, P.; Eisenberger, P. M.; Chidsey, C. E., Alkyl Monolayers on Silicon Prepared from 1-Alkenes and Hydrogen-Terminated Silicon. *J. Am. Chem. Soc.* **1995**, *117*, 3145-3155.

16. Linford, M. R.; Chidsey, C. E., Alkyl Monolayers Covalently Bonded to Silicon Surfaces. *J. Am. Chem. Soc.* **1993**, *115*, 12631-12632.

17. Cicero, R. L.; Linford, M. R.; Chidsey, C. E., Photoreactivity of Unsaturated Compounds with Hydrogen-Terminated Silicon (111). *Langmuir* **2000**, *16*, 5688-5695.

18. Buriak, J. M., Organometallic Chemistry on Silicon and Germanium Surfaces. *Chem. Rev.* **2002**, *102*, 1271-1308.

19. Chai, J.; Wang, D.; Fan, X.; Buriak, J. M., Assembly of Aligned Linear Metallic Patterns on Silicon. *Nat. Nanotechnol* **2007**, *2*, 500-506.

20. Sun, Q. Y.; de Smet, L. C.; van Lagen, B.; Wright, A.; Zuilhof, H.; Sudhölter, E. J., Covalently Attached Monolayers on Hydrogen-Terminated Si (100): Extremely Mild Attachment by Visible Light. *Angew. Chem.* **2004**, *116*, 1376-1379.

21. Fabre, B.; Hauquier, F., Single-Component and Mixed Ferrocene-Terminated Alkyl Monolayers Covalently Bound to Si (111) Surfaces. *J. Phys. Chem. B* **2006**, *110*, 6848-6855.

22. Fabre, B.; Lopinski, G. P.; Wayner, D. D., Photoelectrochemical Generation of Electronically Conducting Polymer-Based Hybrid Junctions on Modified Si (111) Surfaces. *J. Phys. Chem. B* **2003**, *107*, 14326-14335.

23. Piotto, C.; Pujari, S. P.; Zuilhof, H.; Bettotti, P., Surface Heterogeneous Nucleation-Mediated Release of Beta-Carotene from Porous Silicon. *Nanomater.* **2020**, *10*, 1659.

24. Peiris, C. R.; Vogel, Y. B.; Le Brun, A. P.; Aragonès, A. C.; Coote, M. L.; Díez-Pérez, I.; Ciampi, S.; Darwish, N., Metal–Single-Molecule–Semiconductor Junctions Formed by a Radical Reaction Bridging Gold and Silicon Electrodes. *J. Am. Chem. Soc.* **2019**, *141*, 14788-14797.

25. Soria, F. A.; Paredes-Olivera, P.; Patrito, E. M., Chemical Stability toward O2 and H2o of Si (111) Grafted with□ Ch3,□ Ch2ch2ch3,□ Chchch3, and□ Ccch3. *J. Phys. Chem. C* **2015**, *119*, 284-295.

26. Popoff, R. T.; Asanuma, H.; Yu, H.-Z., Long-Term Stability and Electrical Performance of Organic Monolayers on Hydrogen-Terminated Silicon. *J. Phys. Chem. C* **2010**, *114*, 10866-10872.

27. Rosso-Vasic, M.; Spruijt, E.; Van Lagen, B.; De Cola, L.; Zuilhof, H., Alkyl-Functionalized Oxide-Free Silicon Nanoparticles: Synthesis and Optical Properties. *Small* **2008**, *4*, 1835-1841.

28. Shah, A.; Schade, H.; Vanecek, M.; Meier, J.; Vallat-Sauvain, E.; Wyrsch, N.; Kroll, U.; Droz, C.; Bailat, J., Thin-Film Silicon Solar Cell Technology. *Prog. Photovolt.: Res. Appl.* **2004**, *12*, 113-142.

29. Wang, J.; Wu, F.; Watkinson, M.; Zhu, J.; Krause, S., "Click" Patterning of Self-Assembled Monolayers on Hydrogen-Terminated Silicon Surfaces and Their Characterization Using Light-Addressable Potentiometric Sensors. *Langmuir* **2015**, *31*, 9646-9654.

30. Goncales, V. R.; Lian, J.; Gautam, S.; Hagness, D.; Yang, Y.; Tilley, R. D.; Ciampi, S.; Gooding, J. J., Heterojunctions Based on Amorphous Silicon: A Versatile Surface Engineering Strategy to Tune Peak Position of Redox Monolayers on Photoelectrodes. *J. Phys. Chem. C* **2019**, *124*, 836-844.

31. Stewart, M. P.; Buriak, J. M., Chemical and Biological Applications of Porous Silicon Technology. *Adv. Mater.* **2000**, *12*, 859-869.

32. Trilling, A. K.; Beekwilder, J.; Zuilhof, H., Antibody Orientation on Biosensor Surfaces: A Minireview. *Analyst* **2013**, *138*, 1619-1627.

33. Wang, J.; Yang, Z.; Chen, W.; Du, L.; Jiao, B.; Krause, S.; Wang, P.; Wei, Q.; Zhang, D.-W.; Wu, C., Modulated Light-Activated Electrochemistry at Silicon Functionalized with Metal-Organic Frameworks Towards Addressable DNA Chips. *Biosens. Bioelectron.* **2019**, *146*, 111750.

34. Canham, L. T.; Reeves, C. L.; Newey, J. P.; Houlton, M. R.; Cox, T. I.; Buriak, J. M.; Stewart, M. P., Derivatized Mesoporous Silicon with Dramatically Improved Stability in Simulated Human Blood Plasma. *Adv. Mater.* **1999**, *11*, 1505-1507.

35. Fabre, B.; Hauquier, F.; Herrier, C.; Pastorin, G.; Wu, W.; Bianco, A.; Prato, M.; Hapiot, P.; Zigah, D.; Prasciolu, M., Covalent Assembly and Micropatterning of Functionalized Multiwalled Carbon Nanotubes to Monolayer-Modified Si (111) Surfaces. *Langmuir* **2008**, *24*, 6595-6602.

36. Rahpeima, S.; Dief, E. M.; Peiris, C. R.; Ferrie, S.; Duan, A.; Ciampi, S.; Raston, C. L.; Darwish, N., Reduced Graphene Oxide–Silicon Interface Involving Direct Si–O Bonding as a Conductive and Mechanical Stable Ohmic Contact. *Chem. Commun.* **2020**, *56*, 6209-6212.

37. Buriak, J. M., Organometallic Chemistry on Silicon Surfaces: Formation of Functional Monolayers Bound through Si–C Bonds. *Chem. Commun.* **1999**, 1051-1060.

38. Aragones, A. C.; Darwish, N.; Ciampi, S.; Sanz, F.; Gooding, J. J.; Díez-Pérez, I., Single-Molecule Electrical Contacts on Silicon Electrodes under Ambient Conditions. *Nat. Commun.* **2017**, *8*, 1-8.

39. Wu, F.; Zhang, D.-W.; Wang, J.; Watkinson, M.; Krause, S., Copper Contamination of Self-Assembled Organic Monolayer Modified Silicon Surfaces Following a “Click” Reaction Characterized with Laps and Spim. *Langmuir* **2017**, *33*, 3170-3177.

40. Popoff, R. T.; Zavareh, A. A.; Kavanagh, K. L.; Yu, H.-Z., Reduction of Gold Penetration through Phenyl-Terminated Alkyl Monolayers on Silicon. *J. Phys. Chem. C* **2012**, *116*, 17040-17047.

41. Wang, J.; Zhou, Y.; Watkinson, M.; Gautrot, J.; Krause, S., High-Sensitivity Light-Addressable Potentiometric Sensors Using Silicon on Sapphire Functionalized with Self-Assembled Organic Monolayers. *Sens. Actuators B Chem.* **2015**, *209*, 230-236.

42. Fabre, B., Ferrocene-Terminated Monolayers Covalently Bound to Hydrogen-Terminated Silicon Surfaces. Toward the Development of Charge Storage and Communication Devices. *Acc. Chem. Res.* **2010**, *43*, 1509-1518.

43. Jia, C.; Guo, X., Molecule–Electrode Interfaces in Molecular Electronic Devices. *Chem. Soc. Rev.* **2013**, *42*, 5642-5660.

44. Rahpeima, S.; Dief, E. M.; Ciampi, S.; Raston, C. L.; Darwish, N., Impermeable Graphene Oxide Protects Silicon from Oxidation. *ACS Appl. Mater. Interfaces* **2021**.

45. Dief, E. M.; Vogel, Y. B.; Peiris, C. R.; Le Brun, A. P.; Gonçales, V. R.; Ciampi, S.; Reimers, J. R.; Darwish, N., Covalent Linkages of Molecules and Proteins to Si–H Surfaces Formed by Disulfide Reduction. *Langmuir* **2020**, *36*, 14999-15009.

46. Sieval, A. B.; Vleeming, V.; Zuilhof, H.; Sudhölter, E. J., An Improved Method for the Preparation of Organic Monolayers of 1-Alkenes on Hydrogen-Terminated Silicon Surfaces. *Langmuir* **1999**, *15*, 8288-8291.

47. Terry, J.; Linford, M. R.; Wigren, C.; Cao, R.; Pianetta, P.; Chidsey, C. E., Alkyl-Terminated Si (111) Surfaces: A High-Resolution, Core Level Photoelectron Spectroscopy Study. *J. Appl. Phys.* **1999**, *85*, 213-221.

48. Sieval, A., Linke. R.; Zuilhof. H.; Sudhölter, Ejr. *Adv. Mater* **2000**, *12*, 1457-1460.

49. Munkholm, A.; Brennan, S., Ordering in Thermally Oxidized Silicon. *Phys. Rev. Lett.* **2004**, *93*, 036106.

50. Boukherroub, R.; Morin, S.; Sharpe, P.; Wayner, D. D.; Allongue, P., Insights into the Formation Mechanisms of Si− or Monolayers from the Thermal Reactions of Alcohols and Aldehydes with Si (111)− H1. *Langmuir* **2000**, *16*, 7429-7434.

51. Boukherroub, R.; Morin, S.; Bensebaa, F.; Wayner, D., New Synthetic Routes to Alkyl Monolayers on the Si (111) Surface1. *Langmuir* **1999**, *15*, 3831-3835.

52. Fabre, B., Functionalization of Oxide-Free Silicon Surfaces with Redox-Active Assemblies. *Chem. Rev.* **2016**, *116*, 4808-4849.

53. Scheres, L.; Giesbers, M.; Zuilhof, H., Organic Monolayers onto Oxide-Free Silicon with Improved Surface Coverage: Alkynes Versus Alkenes. *Langmuir* **2010**, *26*, 4790-4795.

54. Scheres, L.; Rijksen, B.; Giesbers, M.; Zuilhof, H., Molecular Modeling of Alkyl and Alkenyl Monolayers on Hydrogen-Terminated Si (111). *Langmuir* **2011**, *27*, 972-980.

55. Seitz, O.; Fernandes, P. G.; Tian, R.; Karnik, N.; Wen, H.-C.; Stiegler, H.; Chapman, R. A.; Vogel, E. M.; Chabal, Y. J., Control and Stability of Self-Assembled Monolayers under Biosensing Conditions. *J. Mater. Chem.* **2011**, *21*, 4384-4392.

56. Flynn, N. T.; Tran, T. N. T.; Cima, M. J.; Langer, R., Long-Term Stability of Self-Assembled Monolayers in Biological Media. *Langmuir* **2003**, *19*, 10909-10915.

57. Vogel, Y. B.; Molina, A.; Gonzalez, J.; Ciampi, S., Quantitative Analysis of Cyclic Voltammetry of Redox Monolayers Adsorbed on Semiconductors: Isolating Electrode Kinetics, Lateral Interactions, and Diode Currents. *Anal. Chem.* **2019**, *91*, 5929-5937.

58. Vogel, Y. B.; Zhang, L.; Darwish, N.; Gonçales, V. R.; Le Brun, A.; Gooding, J. J.; Molina, A.; Wallace, G. G.; Coote, M. L.; Gonzalez, J., Reproducible Flaws Unveil Electrostatic Aspects of Semiconductor Electrochemistry. *Nat. Commun.* **2017**, *8*, 1-9.

59. Ciampi, S.; Eggers, P. K.; Le Saux, G.; James, M.; Harper, J. B.; Gooding, J. J., Silicon (100) Electrodes Resistant to Oxidation in Aqueous Solutions: An Unexpected Benefit of Surface Acetylene Moieties. *Langmuir* **2009**, *25*, 2530-2539.

60. Ciampi, S.; Eggers, P. K.; Le Saux, G.; James, M.; Harper, J. B.; Gooding, J. J. J. L., Silicon (100) Electrodes Resistant to Oxidation in Aqueous Solutions: An Unexpected Benefit of Surface Acetylene Moieties. **2009**, *25*, 2530-2539.

61. Ciampi, S.; Böcking, T.; Kilian, K. A.; James, M.; Harper, J. B.; Gooding, J. J. J. L., Functionalization of Acetylene-Terminated Monolayers on Si (100) Surfaces: A Click Chemistry Approach. **2007**, *23*, 9320-9329.

62. Cerofolini, G.; Galati, C.; Renna, L., Accounting for Anomalous Oxidation States of Silicon at the Si/Sio2 Interface. *Surface and Interface Analysis: An International Journal devoted to the development and application of techniques for the analysis of surfaces, interfaces and thin films* **2002**, *33*, 583-590.

63. Cerofolini, G.; Galati, C.; Reina, S.; Renna, L., Quantitative Xps Analysis of Hydrosilated 1-Alkene and 1-Alkyne at Terraced, Dihydrogen-Terminated, 1× 1 (100) Silicon. *Surface and Interface Analysis: An International Journal devoted to the development and application of techniques for the analysis of surfaces, interfaces and thin films* **2006**, *38*, 126-138.

64. Scheres, L.; Arafat, A.; Zuilhof, H., Self-Assembly of High-Quality Covalently Bound Organic Monolayers onto Silicon. *Langmuir* **2007**, *23*, 8343-8346.

65. Barsukov, Y.; Macdonald, J. R., Electrochemical Impedance Spectroscopy. *Mater. Charact.* **2012**, *2*, 898-913.

66. Engelhardt, G. R.; Case, R. P.; Macdonald, D. D., Electrochemical Impedance Spectroscopy Optimization on Passive Metals. *J. Electrochem. Soc.* **2016**, *163*, C470.

67. Macdonald, J. R.; Potter Jr, L. D., A Flexible Procedure for Analyzing Impedance Spectroscopy Results: Description and Illustrations. *Solid State Ionics* **1987**, *24*, 61-79.

68. Macdonald, J. R., Impedance Spectroscopy. *Annals of biomedical engineering* **1992**, *20*, 289-305.

69. Ciampi, S.; Choudhury, M. H.; Ahmad, S. A. B. A.; Darwish, N.; Le Brun, A.; Gooding, J. J., The Impact of Surface Coverage on the Kinetics of Electron Transfer through Redox Monolayers on a Silicon Electrode Surface. *Electrochim. Acta* **2015**, *186*, 216-222.

TOC graphic